Article

Archimedean Spirals with Controllable Chirality: Disk Substrate-Mediated Solution Assembly of Rod−Coil Block Copolymers

Chunhua Cai, Hongfeng Tang, Feiyan Li, Zhanwen Xu,* Jiaping Lin,* Da Li, Zhengmin Tang, Chunming Yang, and Liang Gao

Cite This: *JACS Au* 2024, 4, 2363−2371

Read Online

ACCESS | Metrics & More | Article Recommendations | Supporting Information

ABSTRACT: Spirals are common in nature; however, they are rarely observed in polymer self-assembly systems, and the formation mechanism is not well understood. Herein, we report the formation of two-dimensional (2D) spiral patterns via microdisk substrate-mediated solution self-assembly of polypeptide-based rod−coil block copolymers. The spiral pattern consists of multiple strands assembled from the block copolymers, and two central points are observed. The spirals fit well with the Archimedean spiral model, and their chirality is dependent on the chirality of the polypeptide blocks. As revealed by a combination of experiments and theoretical simulations, these spirals are induced by an interplay of the parallel ordering tendency of the strands and circular confinement of the microdisks. This work presents the first example regarding substrate-mediated self-assembly of block copolymers into spirals. The gained information could not only enhance our understanding of natural spirals but also assist in both the controllable preparations and applications of spiral nanostructures.

KEYWORDS: *Archimedean spiral, microdisk substrate, rod−coil block copolymer, self-assembly, theoretical simulation*
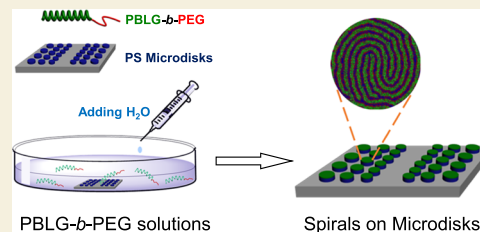
INTRODUCTION

Spiral is a chiral line, which emanates from center points and moves farther away, as it revolves around the point. The well-known forms include arithmetic spirals (Archimedean spirals) and logarithmic spirals.[1−3] Both two-dimensional (2D) and three-dimensional (3D) forms of spirals are observed in nature, such as fingerprints, hair whorls, cobwebs, typhoon tracks, and star trajectories. Spirals have gained long-standing research interests. Many efforts have been devoted to seeking the structure characteristic, the formation mechanism, and their roles playing in nature phenomena.[4−9] Recently, spiral structures have also attracted attentions for their broad range of potential applications in diverse fields including bionics, sensors, and microelectronics industry.[10−13]

Polymers are capable of self-assembling into diverse nanostructures,[14−19] however, spiral nanostructures are barely observed and the knowledge for the formation of spirals is limited.[20−22] It is desirable to explore the inherent controlling factors and find feasible self-assembly methods toward polymer spiral nanostructures. Polymer film self-assembly restricted on a circular confinement could lead to spiral nanostructures, however, concentric toroids rather than spirals are formed in most cases.[23−28] Recently, substrate-mediated solution self-assembly of polymers has become a feasible way to prepare diverse surface nanostructures.[29−35] For example, Zhao et al. found that block copolymers physically trapped on microspheres can self-assemble into spherical and cylindrical surface micelles.[29] Lin et al. have studied the self-assembly behavior of polypeptide-based block copolymers in the presence of various

substrates. For example, they found that poly(γ-benzyl-L-glutamate)-*block*-poly(ethylene glycol) rod−coil block copolymers can self-assemble into nanostrands on nanocylinders,[31−33] nanotoroids,[34] microspheres,[22] and plain surface.[35] The substrate-mediated solution self-assembly of polymers is a promising way to generate novel nanostructures.

Herein, we report that through microdisk substrate-mediated solution self-assembly, PBLG-*b*-PEG rod−coil block copolymers are capable of assembling into nanostrands that form clockwise Archimedean spirals with two centers. The analysis of the characteristic features of the spirals shows that the distance between the two center points, the turning rate, and the strand number depends on the size of the disk substrates. The spiral pattern was found to be energy-favorable as compared with other possible patterns such as concentric toroids, as revealed by theoretical simulations. On the basis of the experiments and theoretical simulations, the formation mechanism is revealed. Both the confinement of the disk substrate and parallelly ordering tendency of the polypeptide strands are ascertained to the formation of the Archimedean spirals.

Scheme 1. (a) Schematic Illustration for the Preparation of PS Microdisks by Using a Solvent Evaporation-Driven Self-Assembly Process. (b) Schematic Illustration for the Preparation of Spirals by Self-Assembling PBLG-*b*-PEG on PS Microdisks
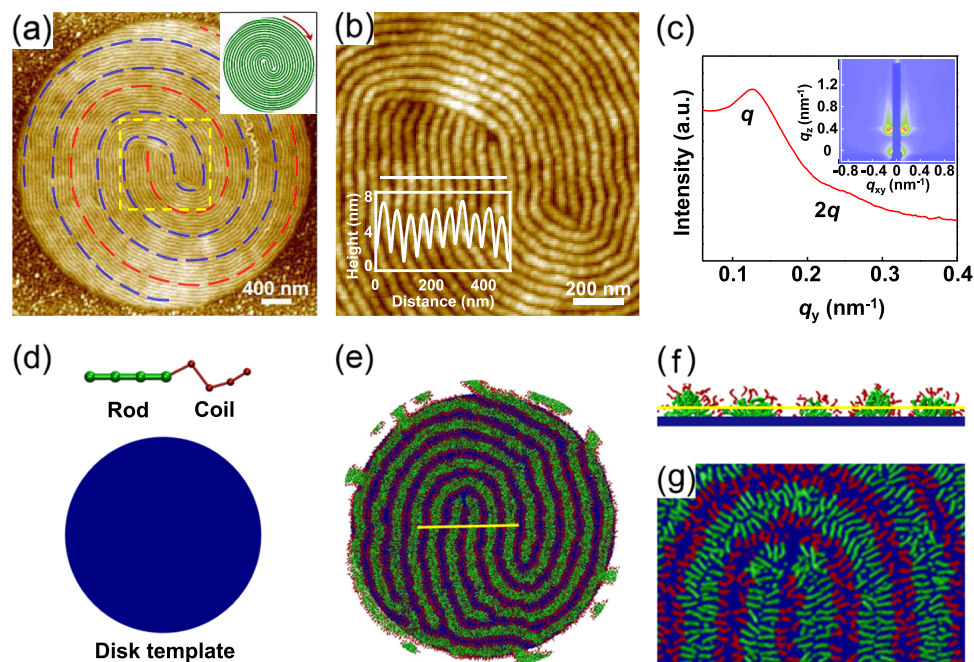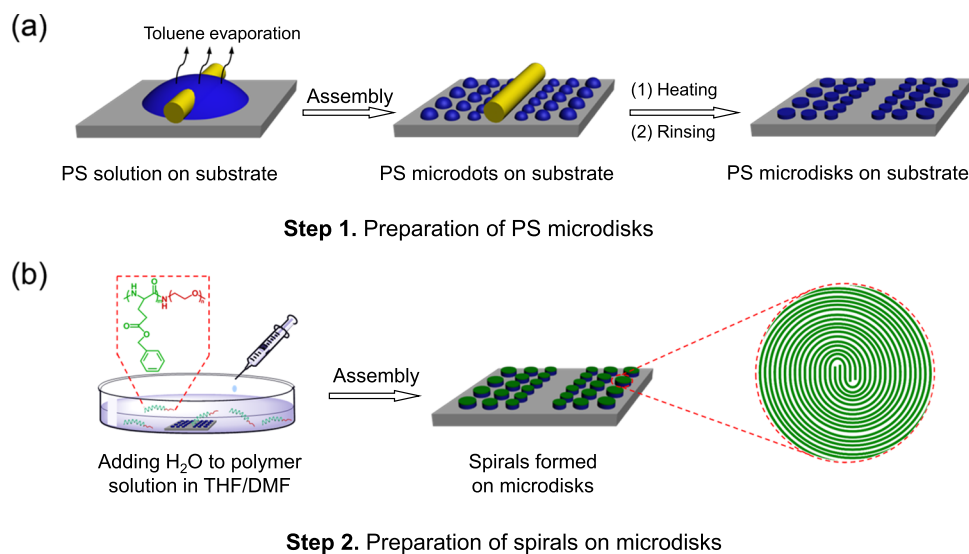

Step 1. Preparation of PS microdisks

Step 2. Preparation of spirals on microdisks

Figure 1. (a) AFM topographic images of the clockwise spirals self-assembled from PBLG$_{55}$-*b*-PEG$_{112}$ BCPs on microdisks with $D = 3.80$ μm. The blue and red dotted lines represent different spiral strands. The inset is a scheme for the double-centered clockwise spiral pattern. (b) Enlarged T-junction grain boundary area of the spirals in panel (a). The inset is the height profile over a scanning distance (white line) of the spirals. (c) 1D profile of the GISAXS pattern. The inset is a 2D GISAXS pattern of the spirals. (d−g) Simulations results: (d) Simulation models of R$_4$-*b*-C$_4$ rod−coil block copolymer and disk. (e) Typical spirals reproduced by DPD simulations. (f) The cross-sectional image of the spirals along the yellow line in panel (e). (g) The cross-sectional image of the spirals along the yellow line in panel (f).

RESULTS AND DISCUSSION

Morphology and Structure of the Spirals

A two-step preparation process for the spirals is illustrated in Scheme 1. First (Step 1), polystyrene (PS) microdisks were prepared by a solvent evaporation-driven self-assembly method.[36,37] Briefly, a drop of dilute PS toluene solution (1 wt %) was confined in a Cu cylinder-on-Si substrate to form a capillary-held microfluid. With the evaporation of toluene, the PS homopolymers assemble into dots with diameters ranging from 1 to 5 μm on the Si substrate due to the "coffee ring"

effect and Rayleigh instability. After thermal annealing and rinsing with toluene, the ultrathin PS microdisks (thickness is about 12 nm), which are stable in common organic solvents, are obtained.[38−40] The details for the preparation of PS microdisks are available in Section 1.3 of the Supporting Information.

In Step 2, the microdisks are used as templates mediating self-assembly of the poly(γ-benzyl-L-glutamate)-*block*-poly-(ethylene glycol) (PBLG-*b*-PEG) block copolymers (BCPs) in solution. Typically, to a solution of PBLG$_{55}$-*b*-PEG$_{112}$ (the subscripts denote the degree of polymerization, DP, for each

block) in a tetrahydrofuran/N,N-dimethylformamide (THF/DMF) mixture solvent (7/3 in volume), the PS disk-patterned Si substrate was immersed, holding the disk-patterned side upward. Then, water was added to induce the self-assembly of the PBLG-b-PEG BCPs. Finally, the disk-patterned substrate was taken out and rinsed with plenty of water to remove the organic solvents. Atomic force microscopy (AFM) and grazing-incidence small-angle X-ray scattering (GISAXS) were used to characterize the assembly structures. Experimental details for the self-assembly are provided in Section 1.4 of the Supporting Information.

We first examined the morphology of the surface patterns by AFM. As shown in Figure 1a, a fingerprint-like spiral pattern is formed on the disk with a diameter of 3.80 μm. In the center area of the spiral pattern, two centers are clearly observed, and the distance between the two centers (d_{center}) is 0.82 μm. As indicated by the red and blue lines, the strands originate from the center areas, and each strand revolves about two turns away from the center to the edge of the disk. The number of strands between two successive turns is defined as the strand number (n), which is 27 on average for the present spiral pattern. In addition, from the revolution direction of the strands from the edge to the center, identical clockwise handedness of the spirals is recognized. PBLG is a helical polymers,[41] and the origin of the homochirality of the spirals is believed to be related to the chiral characteristic of the PBLG blocks. A scheme for the double-centered clockwise spiral pattern with multistrands is given in the inset of Figure 1a.

Figure 1b shows an enlarged image of the center areas (as indicated by the yellow square in Figure 1a) and the height profile of the strands. Two T-junction grains are clearly observed in which some of the strands generated from different grains connect with each other forming reverse S-shaped curves. The height profile (inset in Figure 1b) reveals that these tightly packed spiral strands have a nearly identical diameter of about 48 nm. As can be seen from Figure 1a,b, the spiral strands are tightly packed with each other; therefore, the pitch defined as the distance between the adjacent strands is equal to the diameter of the strands (pitch ≈48 nm).

The periodical structure of the patterns was further confirmed by GISAXS testing, which is a powerful tool to gain the ordered information of nanostructures on surfaces.[42−44] The results are presented in Figure 1c. An apparent scattering spot on the 2D GISAXS pattern is observed (inset of Figure 1c), confirming the existence of periodicity nanostructures. From the one-dimensional (1D) profile along the y-direction (Figure 1c), a characteristic scattering peak at q = 0.129 nm^{-1} is observed, which corresponds to the periodicity of 48.8 nm along the in-plane plane of the disks. The GISAXS results are well consistent with the AFM observations.

Since the self-assembly of PBLG-b-PEG BCPs occurs at an interface between the hydrophobic substrate and solutions, these strands can be termed surface cylindrical micelles.[34,45,46] As characterized by AFM testing (Figures S2 and S3), the height of these spirals is about 4 nm, which is much smaller than the length of PBLG blocks (the length of PBLG$_{55}$ blocks is about 8.2 nm[46]). The BCPs should lie down on the substrate rather than stand on the substrate. Due to the rigid nature of PBLG blocks, these BCPs prefer to pack parallel with their long axis perpendicular to the strands. From the radius of the PBLG$_{55}$-b-PEG$_{112}$ spiral strands (about 24 nm), an end-to-end alignment manner of the BCPs in the strands is deduced. Such a packing manner resembles the smectic form of PBLG LCs.[47]

In such a packing manner, the shell of the spirals occupied by PEG$_{112}$ blocks is about 16 nm, which accounts for a reasonable PEG stretching degree of 41% (the full stretched length of PEG$_{112}$ is about 39 nm).[48,49] In addition, considering that the diameter of the PBLG is about 1.4 nm,[22] we can infer that there could be about 4−5 layers of PBLG chains in the spiral strands.

In addition to the experimental observations, we performed dissipative particle dynamics (DPD) simulations on model systems to further explore the inherent structures of the spirals, such as the chain packing manner. In the DPD simulations, a group of atoms or a volume of fluids is represented by the DPD beads, and the pairwise interactions between i and j components of beads are described by the interaction parameter a_{ij}.[50−52] A higher a_{ij} value corresponds to a stronger pairwise repulsion interaction. Herein, coarse-grained models of the block copolymer and disk template are shown in Figure 1d. To simulate PBLG$_{55}$-b-PEG$_{112}$ block copolymers, a R$_4$-b-C$_4$ model chain connected by harmonic bonds was constructed in which the R beads represent the rod PBLG blocks and the C beads denote the coil PEG blocks. The PS disk template was built up by arranging P beads in FCC packing fashion, in which the P beads are packed densely to prevent the beads of copolymers and solvents from permeating through the disk. In addition, the solvent beads (S) are also explicitly included in the simulation systems. According to the experimental conditions, the interaction parameters are set as a_{RS} = 80, a_{CS} = 30, a_{RP} = 30, a_{PS} = 120, and a_{RC} = 80. The simulation details are presented in Section 2 of the Supporting Information.

As shown in Figure 1e, a multistrand double-centered spiral pattern is predicted by the DPD simulations. The inner structures of the strands are shown from the cross-sectional images (Figure 1f,g). In these strands, the hydrophobic rod blocks (PBLG) form the core, and the hydrophilic coils (PEG) wrap outside (Figure 1f). A perpendicular lamella structure formed by the BCPs can be seen in Figure 1g. The rod blocks adhering to the substrate tend to be perpendicular to the strand axis, and they are packed in a head-to-head manner in the core of the surface cylindrical micelles. These simulation results are consistent with that deduced from the experimental observations. Figure S4 represents a scheme for the cross section of the BCP chain packing mode in the spiral strands. The PBLG-b-PEG BCPs lay down on the substrates, they pack parallelly with an end-to-end alignment manner in the strands, and their long axis is perpendicular to the strands.

As illustrated by both the experiments and simulations, the PBLG-b-PEG strands possess constant diameters, and they are tightly packed with each other. Considering that a constant distance between successive strands is one of the essential characteristics of the Archimedean spirals, these spirals are most likely to be Archimedean spirals. To test such an assumption, we used the standard polar equation of the Archimedean spiral to fit the spirals obtained in the experiments. The polar equation of the Archimedean spiral is given by[53,54]

$$r = a\theta + r_0 \tag{1}$$

where r is the polar radius, a is turning rate (angular velocity), which is a constant value relative to the distance between two successive turns (equals to $2\pi a$), and θ is the polar angle, r_0 is a constant corresponding to the polar radius at the starting point
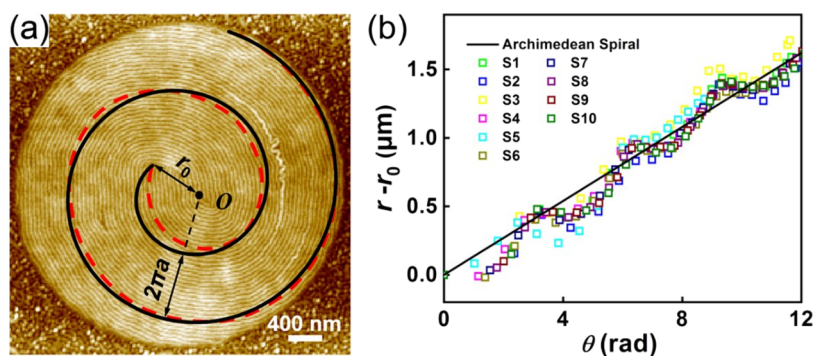
Figure 2. (a) A superimposition of an Archimedean spiral (black curve) on an experimental spiral (red dotted curve). (b) Plot of polar radius $r - r_0$ versus polar angle θ for the spirals. Data from 10 strands numbered S1, S2, ⋯, and S10 are incorporated to plot the $r - r_0$ versus θ trace.
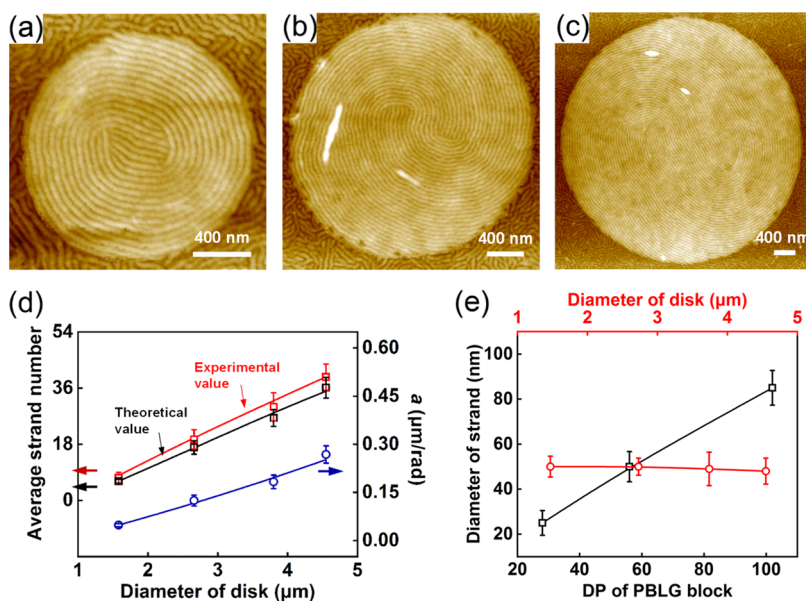

Figure 3. (a–c) AFM images of the spirals formed by $PBLG_{55}$-b-PEG_{112} block copolymers on microdisks with various diameters: (a) 1.58 μm, (b) 2.66 μm, and (c) 4.55 μm. (d) Variation in the average strand number (n) and the average turning rate (a) of the spirals as a function of diameter of the disk. (e) A dependence of diameter of the spirals on size of the disk and DP of the PBLG blocks.

of the spiral where $\theta = 0$. Details of the fitting method are presented in Supporting Information, Section 1.6.

Figure 2a gives a superimposition of an Archimedean spiral (black curve) on an experimental spiral (red dotted curve) formed on a disk with $D = 3.80$ μm. To analyze the relationship between the radii ($r - r_0$) and the polar angle (θ), 10 spiral strands (expressed as S_i, $i = 1-10$) were traced. As shown in Figure 2b, the traces of the strands obtained in the experiments are well-fitted with eq 1, and all of the strand profiles are on a linear regression curve, indicating a good accuracy of the numerical fitting. These results corroborate that the spirals observed in the experiments are Archimedean spirals. The slope of the fitting line gives an average turning rate (a) of the spirals, which is 0.18 μm/rad. The turning rate is associated with the distance between two successive turns (equal to $2\pi a$) of the spirals. From the pitch (ca. 48 nm) and the distance between two successive turns ($2\pi a \approx 1.13$ μm) of the strands, a theoretical strand number (n_{theor}) of 24 is calculated. Such an n_{theor} value matches well with the experimental observations ($n_{exp} = 27$).

Formation Mechanism of the Spirals

The disk confinement is essential for the formation of the spirals. In the absence of disk substrates, the $PBLG_{55}$-b-PEG_{112} BCPs form spherical micelles, which is distinct to the surface cylindrical micelles formed on the disk substrate. To gain deep insight into the formation mechanism of the spirals, the effect of disk size on the morphology of the spiral pattern was examined. As shown in Figure 3a–c, on microdisks with various sizes ($D = 1.58$, 2.66, and 4.55 μm), $PBLG_{55}$-b-PEG_{112} BCPs always form double-centered spiral patterns. The diameters of the strands are similar (Figure 3e). However, these spiral patterns have different structure features. The distance between the two centers (d_{center}) increases with the size of the disk. For the spirals formed on the 1.58 μm disk, the two centers almost merge together ($d_{center} \to 0$). The d_{center} values increase to 0.62 and 1.56 μm for the spirals formed on 2.66 and 4.55 μm disks, respectively. The n_{exp} value of the spirals continuously increases from 6 to 36 when the diameter of the disks increases from 1.58 to 4.55 μm. The dependence of the a and n_{theor} values on the size of the disks was also analyzed. As shown in Figure 3d, with the diameter of the disks increasing from 1.58 to 4.55 μm, the a value increases linearly
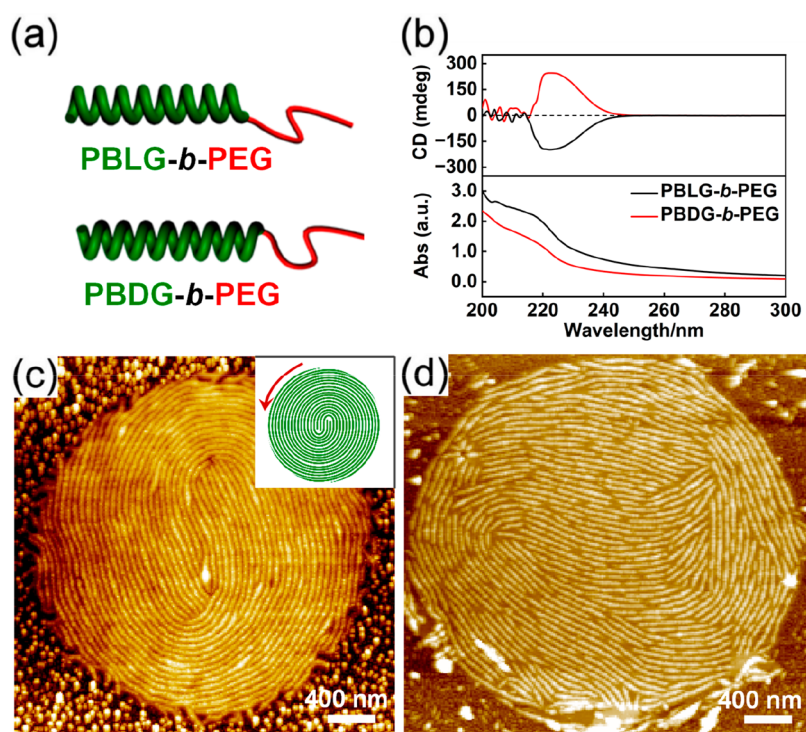
Figure 4. (a) Structures of PBLG-*b*-PEG (PBLG: right-handed α-helix) and PBDG-*b*-PEG (PBDG: left-handed α-helix) block copolymers. (b) CD and UV–vis spectra of PBLG$_{55}$-*b*-PEG$_{112}$ and PBDG$_{55}$-*b*-PEG$_{112}$ block copolymers. (c) Anticlockwise spirals formed by PBDG$_{55}$-*b*-PEG$_{112}$ block copolymers on a microdisk. The inset is a scheme for the anticlockwise spiral pattern. (d) Irregular pattern formed by PBLG$_{55}$-*b*-PEG$_{112}$/PBDG$_{55}$-*b*-PEG$_{112}$ mixtures on a microdisk.

from 0.048 to 0.27 μm/rad, correspondingly, the n_{theor} value increases from 6 to 34. The n_{theor} values are close to the n_{exp} values obtained from the AFM observations. It should be noted that on a large plain PS substrate ($D \rightarrow \infty$), the PBLG-*b*-PEG strands are much straighter, and they prefer to pack with each other in a parallel way forming a large-scale ordered stripe nanopattern (Figure S5).[55] Therefore, the results gained in this work suggest that the presence of a microdisk is a necessary condition for enabling the formation of a spiral structure by PBLG-*b*-PEG BCPs.

The length of the PBLG block also significantly affects the morphology of the surface pattern. It was found that PBLG-*b*-PEG BCPs with various PBLG block lengths can form nanostrands on microdisk substrates (in the absence of the disk substrates, they all form spherical micelles). As shown in Figure 3e, the diameter of the nanostrands increases linearly with the DP of PBLG blocks, that is, from 25 nm for PBLG$_{28}$-*b*-PEG$_{112}$ strands to 48 nm for PBLG$_{55}$-*b*-PEG$_{112}$ strands then to 85 nm for PBLG$_{101}$-*b*-PEG$_{112}$ strands. These nanostrands formed by different BCPs generated different surface patterns. The BCPs with short PBLG blocks (PBLG$_{28}$-*b*-PEG$_{112}$) form spirals on microdisks (Figure S6a, disk size of D = 2.1 μm). The d_{center} and n_{exp} values are 0.43 and 9, respectively. Numerical fitting analysis reveals that the values of n_{theor} and a are 10 and 0.041 μm/rad, respectively. The BCPs with long PBLG blocks, for example, PBLG$_{101}$-*b*-PEG$_{112}$, form relatively straight strands that are randomly dispersed on the disk (no spiral pattern can be observed, Figure S6c). It should be noted that these BCPs used in this study have relatively small molecular weight distribution ($Đ < 1.27$); when BCPs with a large $Đ$ value ($Đ = 1.38$), ill-defined strands are formed. Therefore, the formation of well-defined spiral patterns requires a suitable length for the PBLG blocks. These results

also indicate that the thinner spirals formed by the BCPs with shorter PBLG blocks have a smaller turning rate and fewer strand numbers (that is, the thinner strands are curved to a higher degree). Additionally, the rigidity of the polypeptide blocks is essential for the formation of spiral patterns. For example, when replacing PBLG-*b*-PEG rod–coil BCPs with PS-*b*-PEG coil–coil BCPs, no apparent pattern on the PS disks was observed (Figure S7).

As mentioned above, the PBLG-*b*-PEG spirals possess clockwise handedness (see Figures 1 and 3). It is well-known that chirality can transfer between different levels, such as from molecular to supramolecular structures. Under certain conditions, it can also be inhibited. PBLG is a helical polymer, and its backbone takes a right-handed α-helix conformation. Upon the formation of spirals, chirality transfer occurs from the polymers to the spirals, which results in clockwise handedness. It is known that poly(γ-benzyl-D-glutamate) (PBDG) is an enantiomer to PBLG, which takes an opposite chirality to PBLG.[34,41] Figure 4a shows the structures of PBLG-*b*-PEG and PBDG-*b*-PEG BCPs. The opposite chirality of PBLG and PBDG was confirmed by ultraviolet–visible (UV–vis) and circular dichroism (CD) testing (Figure 4b). In the UV–vis spectrum, an evident absorption around 220 nm was observed, indicating that optically active groups are present in polypeptides. PBLG-*b*-PEG (PBDG-*b*-PEG) BCPs display negative (positive) Cotton effect as revealed by the CD spectrum in the similar position. The negative Cotton effect indicates right-handed PBLG blocks, while the positive Cotton effect means left-handed chirality of the PBDG blocks.

When the PBLG-*b*-PEG BCPs are replaced by PBDG-*b*-PEG BCPs in the preparation of spiral samples, as expected, the PBDG-*b*-PEG BCPs form anticlockwise spirals under similar conditions. Figure 4c shows the anticlockwise spirals
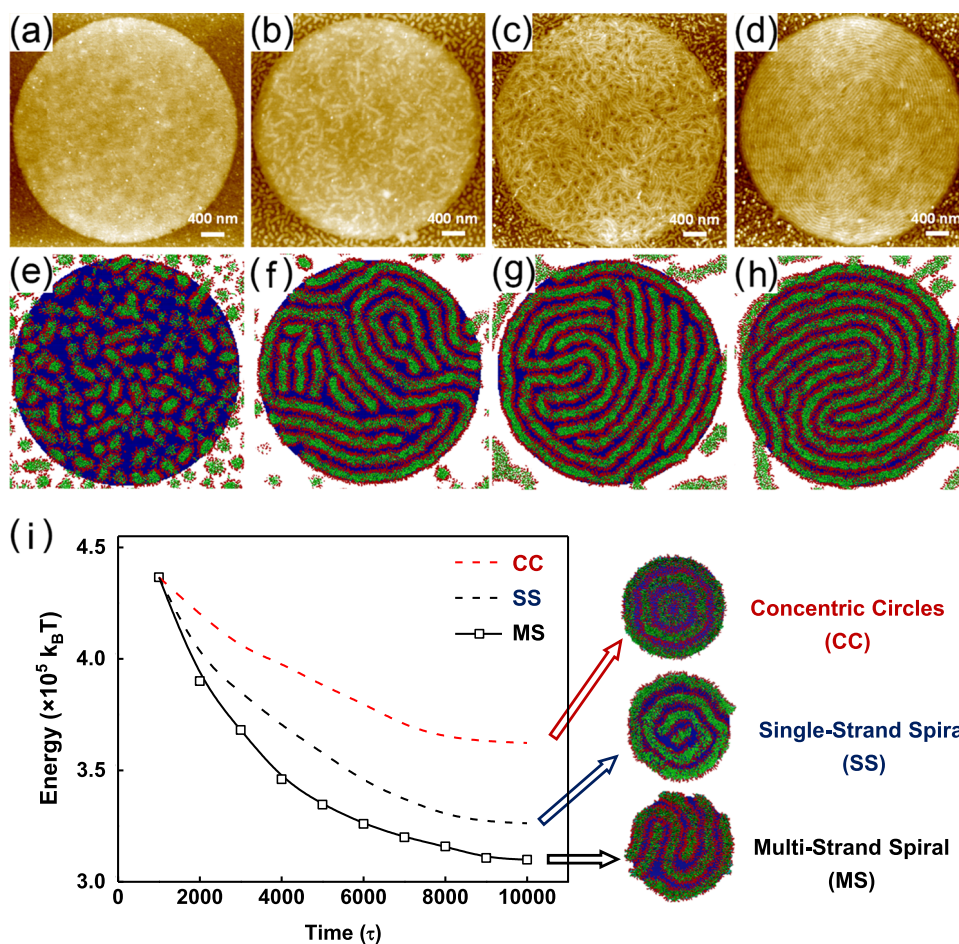
Figure 5. (a–d) AFM topographic images of PBLG-*b*-PEG self-assembled on microdisks with various added water contents: (a) 12.0 vol %, (b) 17.3 vol %, (c) 22.7 vol %, and (d) 28.0 vol %. (e–h) Stable aggregates on disks obtained from DPD simulations at various solvent conditions: (e) small micelles ($a_{RS} = 35$), (f) short strands ($a_{RS} = 50$), (g) long strands ($a_{RS} = 65$), and (h) multistranded spirals ($a_{RS} = 80$). (i) Energy change of different types of patterns as a function of simulation time.

assembled by the PBDG$_{55}$-*b*-PEG$_{112}$ BCPs on a 2.82 μm disk. The diameter of these PBDG-*b*-PEG strands is uniform (about 48 nm), and n_{exp} is 21. These spiral strands can also be fitted with the Archimedean spiral model, and the theoretical strand number (n_{theor}) and turning rate (a) are 19 and 0.15 μm/rad, respectively. Moreover, when PBLG$_{55}$-*b*-PEG$_{112}$ and PBDG$_{55}$-*b*-PEG$_{112}$ BCPs mixtures (1:1 in weight) were used, the spiral patterns are disturbed. As can be seen from Figure 4d, no spirals but randomly dispersed strands are observed. The chirality transfer from polymers to strands is inhibited.

These updated experimental observations and numerical analysis clearly reveal the importance of both confinement of the disk and rigid nature of the block copolymers on the formation of the spirals. Due to the rigid nature of the PBLG blocks, the PBLG-*b*-PEG strands prefer to take a relatively straight form (see Figure S5). Under circular confinement, the PBLG-*b*-PEG strands have to curve into spirals. A decrease of the disk size results in spirals with a smaller value of the turning rate, and the strands are more curved and move slower away from the center to the edge. For the strands formed by PBLG-*b*-PEG BCPs with shorter PBLG blocks, they are thinner and more flexible; therefore, they are easier to be curved under circular confinement forming spirals with a smaller turning rate. In addition, the chirality of the polypeptides transfers to the spirals; therefore, chirality of the spirals can be controlled

by the polypeptides. From these results, we can learn that the formation of such spiral patterns depends on a competition between parallelly ordering tendency of the strands and circular confinement of the microdisks.

Dynamic Formation Process of the Spirals

To get a deep understanding of the formation of the spirals, we studied the variation of surface morphology of spirals formed by PBLG-*b*-PEG BCPs under various water addition (Figure 5a–d). At lower water contents, the BCPs dissolve in the solution and no assembly behavior occurs. For example, under 12.0 vol % of water addition, a smooth surface similar to that of the blank disks was observed (Figure 5a). As the water content increases to 17.3 vol %, short strands appeared on the disks (Figure 5b). When the water content reaches 22.7 vol %, as shown in Figure 5c, long strands closely packed with each other were observed. Increasing the water content up to 28.0 vol % produces spiral patterns on the disks (Figure 5d). Further increasing the water content exerts no significant effect on the morphology of the spirals. Finally, after the samples were rinsed with water to remove the organic solvents, stable spiral patterns were obtained.

The main driving force for the self-assembly of PBLG-*b*-PEG BCPs on PS disks can be the hydrophobic–hydrophobic attractions between PS and PBLG segments and the hydrophobic–hydrophilic balance of PBLG and PEG blocks.

With the addition of water, the solubility of the mixture solvent (THF/DMF/H$_2$O) for the PBLG blocks decreases and the PS disks and PBLG blocks become solvophobic. To reduce the exposure of both the PS disks and the PBLG blocks to the solvents, the PBLG-*b*-PEG BCPs adsorb onto the PS disks. When the water content increases, the PBLG-*b*-PEG BCPs further self-assemble into surface cylindrical micelles with the PBLG as the core and the PEG as the shell. Under higher water contents, these strands tightly pack together to fully cover the disks, resulting in the formation of spirals.

The formation process of the spirals was also studied by DPD simulations (Figure 5e−h). To simulate the effect of the water addition process, the interaction parameter a_{RS} between the rod blocks (R beads) and solvents (S beads) is gradually changed from 35 to 80. A larger a_{RS} stands for a stronger repulsion between the rod blocks and solvents, corresponding to the stronger hydrophobicity of the PBLG blocks under higher water contents. As shown in Figure 5e, when a_{RS} is low (a_{RS} = 35), the model R$_4$-*b*-C$_4$ block copolymers form small aggregates randomly dispersed in the simulation box. Under a_{RS} = 50, the small aggregates are adsorbed onto the disks and transform into short strands (Figure 5f). With an increase in a_{RS} to 65, the short strands connect to form long but disordered strands (Figure 5g). Finally, these strands rearrange their alignment, and multistranded spiral structures appear with further increasing a_{RS} to 80 (Figure 5h).

The energy change of the system in the self-assembly process was further analyzed. In the DPD simulations, the energy can be evaluated by the conservative energy between beads *via* $\sum_{i \neq j} a_{ij}(r_{ij} - r_c)^2/2$, where a_{ij} represents the repulsive parameters, r_{ij} is the distance between beads *i* and *j*, and r_c is the cutoff radius.[50−52,55] The conservative energy as a function of the simulation time is plotted in Figure 5i. As can be seen, the system energy gradually decreases during the absorption of copolymers onto the substrate to form the strands. After the simulation time of 8000τ, the energy reaches a stable state, which indicates that the formed multistranded spiral pattern becomes stable. For comparison, we also calculated the energies of other possible nanostructures formed by the BCPs, such as circular toroids and single-strand spirals. The results are shown in Figure 5i. Among these nanostructures, the multistranded spirals possess the lowest energy, indicating that the multistranded spiral is a stable and favorable pattern.

The spiral form, as a kind of helix, is a fundamental geometrical structure in nature, which has drawn significant attention. As an effort to seek the nature of spirals, we revealed that under the confinement of microdisk substrates, polypeptide-based block copolymers are capable of self-assembling into well-defined Archimedean spirals with controllable chirality and structure features. We expect that the gained information could not only pave our steps to in-depth elucidate the formation mechanism of natural chiral structures like spirals formed by natural molecules but also enhance our ability to prepare spiral nanostructures appealing in applications with a wide range.

CONCLUSIONS

In summary, we discovered that through disk substrate-mediated solution self-assembly, PBLG-*b*-PEG BCPs are able to self-assemble into 2D double-centered homochiral Archimedean spirals. The spiral strands are tightly packed with each other, and both the strand number and the turning rate of the spirals depend on the size of the disks as well as the length of the polypeptide blocks. A chirality transfer occurs from the polypeptides to the spiral patterns, and the chirality sense of the spirals can be tuned by the handedness of the polypeptide blocks. As explicated by the combination of experiments and theoretical simulations, the interplay of parallel ordering tendency of the strands and confinement of the microdisk takes responsibility for the formation of the Archimedean spirals.

ASSOCIATED CONTENT

ⓢ Supporting Information

The Supporting Information is available free of charge at https://pubs.acs.org/doi/10.1021/jacsau.4c00324.

> Synthesis and characterization of polymers, preparation, and characterization of PS microdisks; self-assembly method; characterization of nanostructures; fitting method for the spirals; additional experimental results and discussion; simulation method and parameter settings (PDF)

AUTHOR INFORMATION

Corresponding Authors

Zhanwen Xu − *State Key Laboratory of Molecular Engineering of Polymers, Department of Macromolecular Science, Fudan University, Shanghai 200433, China*; Email: xuzhanwen@fudan.edu.cn

Jiaping Lin − *Shanghai Key Laboratory of Advanced Polymeric Materials, Key Laboratory for Ultrafine Materials of Ministry of Education, Frontiers Science Center for Materiobiology and Dynamic Chemistry, School of Materials Science and Engineering, East China University of Science and Technology, Shanghai 200237, China*; ⓞ orcid.org/0000-0001-9633-4483; Email: jlin@ecust.edu.cn

Authors

Chunhua Cai − *Shanghai Key Laboratory of Advanced Polymeric Materials, Key Laboratory for Ultrafine Materials of Ministry of Education, Frontiers Science Center for Materiobiology and Dynamic Chemistry, School of Materials Science and Engineering, East China University of Science and Technology, Shanghai 200237, China*; ⓞ orcid.org/0000-0001-9008-6327

Hongfeng Tang − *Shanghai Key Laboratory of Advanced Polymeric Materials, Key Laboratory for Ultrafine Materials of Ministry of Education, Frontiers Science Center for Materiobiology and Dynamic Chemistry, School of Materials Science and Engineering, East China University of Science and Technology, Shanghai 200237, China*

Feiyan Li − *Shanghai Key Laboratory of Advanced Polymeric Materials, Key Laboratory for Ultrafine Materials of Ministry of Education, Frontiers Science Center for Materiobiology and Dynamic Chemistry, School of Materials Science and Engineering, East China University of Science and Technology, Shanghai 200237, China*

Da Li − *Shanghai Key Laboratory of Advanced Polymeric Materials, Key Laboratory for Ultrafine Materials of Ministry of Education, Frontiers Science Center for Materiobiology and Dynamic Chemistry, School of Materials Science and Engineering, East China University of Science and Technology, Shanghai 200237, China*

Zhengmin Tang − *Department of Laboratory Medicine, the First Affiliated Hospital, College of Medicine, Zhejiang University, Hangzhou 311121, China*

Chunming Yang − *Shanghai Synchrotron Radiation Facility, Shanghai Advanced Research Institute, Chinese Academy of Sciences, Shanghai 201204, China;* orcid.org/0000-0001-8008-3675

Liang Gao − *Shanghai Key Laboratory of Advanced Polymeric Materials, Key Laboratory for Ultrafine Materials of Ministry of Education, Frontiers Science Center for Materiobiology and Dynamic Chemistry, School of Materials Science and Engineering, East China University of Science and Technology, Shanghai 200237, China;* orcid.org/0000-0001-6852-8301

Complete contact information is available at:
https://pubs.acs.org/10.1021/jacsau.4c00324

Author Contributions

CRediT: **Chunhua Cai** conceptualization, formal analysis, funding acquisition, investigation, writing-original draft, writing-review & editing; **Hongfeng Tang** investigation; **Feiyan Li** investigation; **Zhanwen Xu** formal analysis, investigation, writing-original draft; **Jiaping Lin** conceptualization, funding acquisition, supervision, writing-review & editing; **Da Li** investigation; **Zhengmin Tang** investigation; **Chunming Yang** investigation; **Liang Gao** validation.

Notes

The authors declare no competing financial interest.

■ REFERENCES

(1) Bowman, C.; Newell, A. C. Natural Patterns and Wavelets. *Rev. Mod. Phys.* **1998**, *70*, 289−301.

(2) Yashima, E.; Maeda, K.; Iida, H.; Furusho, Y.; Nagai, K. Helical Polymers: Synthesis, Structures, and Functions. *Chem. Rev.* **2009**, *109*, 6102−6211.

(3) Moloney, M. P.; Govan, J.; Loudon, A.; Mukhina, M.; Gun'Ko, Y. K. Preparation of Chiral Quantum Dots. *Nat. Protoc.* **2015**, *10*, 558−573.

(4) Ziegler, J. I.; Haglund, R. F., Jr Plasmonic Response of Nanoscale Spirals. *Nano Lett.* **2010**, *10*, 3013−3018.

(5) Haudin, F.; Cartwright, J. H.; Brau, F.; De Wit, A. Spiral Precipitation Patterns in Confined Chemical Gardens. *Proc. Natl. Acad. Sci. U.S.A.* **2014**, *111*, 17363−17367.

(6) Barada, D.; Juman, G.; Yoshida, I.; Miyamoto, K.; Kawata, S.; Ohno, S.; Omatsu, T. Constructive Spin-Orbital Angular Momentum Coupling Can Twist Materials to Create Spiral Structures in Optical Vortex Illumination. *Appl. Phys. Lett.* **2016**, *108*, 8185−8189.

(7) Golvano-Escobal, I.; Gonzalez-Rosillo, J. C.; Domingo, N.; Illa, X.; López-Barberá, J. F.; Fornell, J.; Solsona, P.; Aballe, L.; Foerster, M.; Suriñach, S.; Baró, M. D.; Puig, T.; Pané, S.; Nogués, J.; Pellicer, E.; Sort, J. Spontaneous Formation of Spirallike Patterns with Distinct Periodic Pphysical Properties by Confined Eelectrodeposition of Co-In Disks. *Sci. Rep.* **2016**, *6*, No. 30398, DOI: 10.1038/srep30398.

(8) Sönmezoğlu, S.; Sönmezoğlu, Ö. A. Optical and Dielectric Properties of Double Helix DNA Thin Films. *Mater. Sci. Eng., C* **2011**, *31*, 1619−1624.

(9) Shaikjee, A.; Coville, N. J. The Synthesis, Properties and Uses of Carbon Materials with Helical Morphology. *J. Adv. Res.* **2012**, *3*, 195−223.

(10) Zhu, W.; Cai, C.; Lin, J.; Wang, L.; Chen, L.; Zhuang, Z. Polymer Micelle-Directed Growth of $BaCO_3$ Spiral Nanobelts. *Chem. Commun.* **2012**, *48*, 8544−8546.

(11) Janes, D. W.; Thode, C. J.; Willson, C. G.; Nealey, P. F.; Ellison, C. J. Light-Activated Replication of Block Copolymer Fingerprint Patterns. *Macromolecules* **2013**, *46*, 4510−4519.

(12) Davidson II, R. B.; Ziegler, J. I.; Vargas, G.; Avanesyan, S. M.; Gong, Y.; Hess, W.; Haglund, R. F., Jr Efficient Forward Second-Harmonic Generation from Planar Archimedean Nanospirals. *Nanophotonics* **2015**, *4*, 108−113.

(13) Kwak, B.; Lee, J.; Lee, J.; Kim, H. S.; Kang, S.; Lee, Y. Spiral Shape Microfluidic Channel for Selective Isolating of Heterogenic Ccirculating Tumor Cells. *Biosens. Bioelectron.* **2018**, *101*, 311−316.

(14) Mai, Y.; Eisenberg, A. Self-Assembly of Block Copolymers. *Chem. Soc. Rev.* **2012**, *41*, 5969−5985.

(15) Cai, J.; Li, C.; Kong, N.; Lu, Y.; Lin, G.; Wang, X.; Yao, Y.; Manners, I.; Qiu, H. Tailored Multifunctional Micellar Brushes via Crystallization-Driven Growth from a Surface. *Science* **2019**, *366*, 1095−1098.

(16) Liu, M.; Zhang, L.; Wang, T. Supramolecular Chirality in Self-Assembled Systems. *Chem. Rev.* **2015**, *115*, 7304−7397.

(17) Lu, Y.; Lin, J.; Wang, L.; Zhang, L.; Cai, C. Self-Assembly of Copolymer Micelles: Higher-Level Assembly for Constructing Hierarchical Structure. *Chem. Rev.* **2020**, *120*, 4111−4140.

(18) Ahmed, E.; Cho, J.; Friedmann, L.; Jang, S. S.; Weck, M. Catalytically Active Multicompartment Micelles. *JACS Au* **2022**, *2*, 2316−2326.

(19) Huang, S.; Yu, H.; Li, Q. Supramolecular Chirality Transfer toward Chiral Aggregation: Asymmetric Hierarchical Self-Assembly. *Adv. Sci.* **2021**, *8*, No. 2002132.

(20) Yuan, J.; Lu, X.; Li, Q.; Lü, Z.; Lu, Q. Reversible Micrometer-Scale Spiral Self-Assembly in Liquid Crystalline Block Copolymer Film with Controllable Chiral Response. *Angew. Chem., Int. Ed.* **2021**, *60*, 12308−12312.

(21) Vacogne, C. D.; Wei, C.; Tauer, K.; Schlaad, H. Self-Assembly of α-Helical Polypeptides into Microscopic and Enantiomorphic Spirals. *J. Am. Chem. Soc.* **2018**, *140*, 11387−11394.

(22) Xu, W.; Xu, Z.; Cai, C.; Lin, J.; Gao, L.; Qi, H.; Lin, S. Spiral- and Meridian-Patterned Spheres Self-Assembled from Block Copolymer/Homopolymer Binary Systems. *Nanoscale* **2021**, *13*, 14016−14022.

(23) Cheng, J. Y.; Rettner, C. T.; Sanders, D. P.; Kim, H. C.; Hinsberg, W. D. Dense Self-Assembly on Sparse Chemical Patterns: Rectifying and Multiplying Lithographic Patterns Using Block Copolymers. *Adv. Mater.* **2008**, *20*, 3155−3158.

(24) Chai, J.; Buriak, J. M. Using Cylindrical Domains of Block Copolymers to Self-Assemble and Align Metallic Nanowires. *ACS Nano* **2008**, *2*, 489−501.

(25) Jeong, S. J.; Kim, J. E.; Moon, H.-S.; Kim, B. H.; Kim, S. M.; Kim, J. B.; Kim, S. O. Soft Graphoepitaxy of Block Copolymer Assembly with Disposable Photoresist Confinement. *Nano Lett.* **2009**, *9*, 2300−2305.

(26) Choi, H. K.; Chang, J.-B.; Hannon, A. F.; Yang, J. K. W.; Berggren, K. K.; Alexander-Katz, A.; Ross, C. A. Nanoscale Spirals by Directed Self-Assembly. *Nano Futures* **2017**, *1*, No. 015001.

(27) Jeon, S.-J.; Yi, G.-R.; Koo, C. M.; Yang, S.-M. Nanostructures Inside Colloidal Particles of Block Copolymer/Homopolymer Blends. *Macromolecules* **2007**, *40*, 8430−8439.

(28) Shi, A.-C.; Li, B. Self-Assembly of Diblock Copolymers under Confinement. *Soft Matter* **2013**, *9*, 1398−1413.

(29) Hou, W.; Feng, Y.; Li, B.; Zhao, H. Coassembly of Linear Diblock Copolymer Chains and Homopolymer Brushes on Silica

Particles: A Combined Computer Simulation and Experimental Study. *Macromolecules* **2018**, *51*, 1894−1904.

(30) Jia, L.; Tong, L.; Liang, Y.; Petretic, A.; Guerin, G.; Manners, I.; Winnik, M. A. Templated Fabrication of Fiber-Basket Polymersomes via Crystallization-Driven Block Copolymer Self-Assembly. *J. Am. Chem. Soc.* **2014**, *136*, 16676−16682.

(31) Cai, C.; Li, Y.; Lin, J.; Wang, L.; Lin, S.; Wang, X.-S.; Jiang, T. Simulation-Assisted Self-Assembly of Multicomponent Polymers into Hierarchical Assemblies with Varied Morphologies. *Angew. Chem., Int. Ed.* **2013**, *52*, 7732−7736.

(32) Cai, C.; Lin, J.; Zhu, X.; Gong, S.; Wang, X.-S.; Wang, L. Superhelices with Designed Helical Structures and Temperature-Stimulated Chirality Transitions. *Macromolecules* **2016**, *49*, 15−22.

(33) Yao, Y.; Gao, L.; Cai, C.; Lin, J.; Lin, S. Supramolecular Polymerization of Polymeric Nanorods Mediated by Block Copolymers. *Angew. Chem., Int. Ed.* **2023**, *62*, No. e202216872.

(34) Xu, P.; Gao, L.; Cai, C.; Lin, J.; Wang, L.; Tian, X. Helical Toroids Self-Assembled from a Binary System of Polypeptide Homopolymer and its Block Copolymer. *Angew. Chem., Int. Ed.* **2020**, *59*, 14281−14285.

(35) Tang, Z.; Gao, L.; Lin, J.; Cai, C.; Yao, Y.; Guerin, G.; Tian, X.; Lin, S. Anchorage-Dependent Living Supramolecular Self-Assembly of Polymeric Micelles. *J. Am. Chem. Soc.* **2021**, *143*, 14684−14693.

(36) Yabu, H.; Shimomura, M. Preparation of Self-Organized Mesoscale Polymer Patterns on a Solid Substrate: Continuous Pattern Formation from a Receding Meniscus. *Adv. Funct. Mater.* **2005**, *15*, 575−581.

(37) Byun, M.; Han, W.; Li, B.; Xin, X.; Lin, Z. An Unconventional Route to Hierarchically Ordered Block Copolymers on a Gradient Patterned Surface through Controlled Evaporative Self-Assembly. *Angew. Chem., Int. Ed.* **2013**, *52*, 1122−1127.

(38) Housmans, C.; Sferrazza, M.; Napolitano, S. Kinetics of Irreversible Chain Adsorption. *Macromolecules* **2014**, *47*, 3390−3393.

(39) Jiang, N.; Shang, J.; Di, X.; Endoh, M. K.; Koga, T. Formation Mechanism of High-Density, Flattened Polymer Nanolayers Adsorbed on Planar Solids. *Macromolecules* **2014**, *47*, 2682−2689.

(40) Vignaud, G.; Chebil, M. S.; Bal, J. K.; Delorme, N.; Beuvier, T.; Grohens, Y.; Gibaud, A. Densification and Depression in Glass Transition Temperature in Polystyrene Thin Films. *Langmuir* **2014**, *30*, 11599−11608.

(41) Abe, A.; Furuya, H. Conformational Characteristics of Polypeptide Chains with Special Focus on the α-Helix-Sense Inversion. In:. In *Modern Applications of Flory's "Statistical Mechanics of Chain Molecules*; Tonelli, A. E.; Patterson, G., Eds.; American Chemical Society: Washington, DC, 2020; Vol. *1356*, Chapter 5, pp 63−87.

(42) Lee, M.; Cho, B.-K.; Zin, W.-C. Supramolecular Structures from Rod-Coil Block Copolymers. *Chem. Rev.* **2001**, *101*, 3869−3892.

(43) Lim, Y.-b.; Moon, K.-S.; Lee, M. Rod-Coil Block Molecules: Their Aqueous Self-Assembly and Biomaterials Applications. *J. Mater. Chem.* **2008**, *18*, 2909−2918.

(44) Olsen, B. D.; Segalman, R. A. Self-Assembly of Rod-Coil Block Copolymers. *Mater. Sci. Eng., R* **2008**, *62*, 37−66.

(45) Warr, G. G. Surfactant Adsorbed Layer Structure at Solid/Solution Interfaces: Impact and Implications of AFM Imaging Studies. *Curr. Opin. Colloid Interface Sci.* **2000**, *5*, 88−94.

(46) Xu, W.; Xu, Z.; Cai, C.; Lin, J.; Zhang, S.; Zhang, L.; Lin, S.; Yao, Y.; Qi, H. Ordered Surface Nanostructures Self-Assembled from Rod-Coil Block Copolymers on Microspheres. *J. Phys. Chem. Lett.* **2019**, *10*, 6375−6381.

(47) Yu, S. M.; Soto, C. M.; Tirrell, D. A. Nanometer-Scale Smectic Ordering of Genetically Engineered Rodlike Polymers: Synthesis and Characterization of Monodisperse Derivatives of Poly(γ-benzyl α,L-glutamate). *J. Am. Chem. Soc.* **2000**, *122*, 6552−6559.

(48) Jeppesen, C.; Wong, J. Y.; Kuhl, T. L.; Israelachvili, J. N.; Mullah, N.; Zalipsky, S.; Marques, C. M. Impact of Polymer Tether Length on Multiple Ligand-Receptor Bond Formation. *Science* **2001**, *293*, 465−468 54.

(49) Sun, B.; Xu, Z.; Tang, Z.; Cai, C.; Lin, J. Dot Nanopattern Self-Assembled from Rod-Coil Block Copolymer on Substrate. *Macromol. Chem. Phys.* **2020**, *221*, No. 2000254.

(50) Guan, Z.; Wang, L.; Zhu, X.; Lin, J. Striped Patterns Self-Assembled from Rod-Coil Diblock Copolymers on Spherical Substrates. *Mater. Chem. Front.* **2017**, *1*, 697−708.

(51) Zhang, Q.; Lin, J.; Wang, L.; Xu, Z. Theoretical Modeling and Simulations of Self-Assembly of Copolymers in Solution. *Prog. Polym. Sci.* **2017**, *75*, 1−30.

(52) Koelman, J. M. V. A.; Hoogerbrugge, P. J. Dynamic Simulations of Hard-Sphere Suspensions under Steady Shear. *Europhys. Lett.* **1993**, *21*, 363−368.

(53) Boccaletti, A.; Pantin, E.; Lagrange, A. M.; Augereau, J. C.; Meheut, H.; Quanz, S. P. Multiple Spiral Patterns in the Transitional Disk of HD 100546. *Astron. Astrophys.* **2013**, *560*, No. A20, DOI: 10.1051/0004-6361/201322365.

(54) Sasaki, N.; Mabesoone, M. F. J.; Kikkawa, J.; Fukui, T.; Shioya, N.; Shimoaka, T.; Hasegawa, T.; Takagi, H.; Haruki, R.; Shimizu, N.; Adachi, S.; Meijer, E. W.; Takeuchi, M.; Sugiyasu, K. Supramolecular Double-Stranded Archimedean Spirals and Concentric Toroids. *Nat. Commun.* **2020**, *11*, No. 3578.

(55) Tang, Z.; Li, D.; Lin, J.; Zhang, L.; Cai, C.; Yao, Y.; Yang, C.; Tian, X. Self-Assembly of Rod-Coil Block Copolymers on a Substrate into Micrometer-Scale Ordered Stripe Nanopatterns. *Polym. Chem.* **2020**, *11*, 7487−7496.